Structural and optical parameters of ZnS_xSe_{1-x} films deposited on quartz substrates by laser ablation

1998 Semicond. Sci. Technol. 13 1446

(http://iopscience.iop.org/0268-1242/13/12/021)

Semicond. Sci. Technol. **13** (1998) 1446–1455. Printed in the UK PII: S0268-1242(98)93842-1

Structural and optical parameters of ZnS_xSe_{1-x} films deposited on quartz substrates by laser ablation

M Ambrico†, D Smaldone†, C Spezzacatena†, V Stagno‡, G Perna§ and V Capozzi§‖

† Istituto Materiali Speciali del CNR, Via S Loja, I-85050 Tito Scalo (PZ), Italy
‡ Dipartimento di Fisica dell'Università and INFN—Sezione di Bari, Via Amendola, I-70126 Bari, Italy
§ Dipartimento di Fisica dell'Università di Bari and Istituto Nazionale di Fisica della Materia, Via Amendola, I-70126 Bari, Italy

Received 1 May 1998, accepted for publication 18 August 1998

Abstract. ZnS_xSe_{1-x} laser ablated films deposited on quartz substrates have been studied in order to obtain information on their structural and optical properties as a function of sulphur concentration (x). Transmittance and reflectance spectra at room temperature were carried out to obtain the energy gap modulation, the absorption coefficient and refractive index. By using the Newton–Raphson algorithm, the values of the real part of the refractive index in the transparent region were deduced including the effect of non-uniformity of the film thickness. The wavelength dependence of n was extrapolated for the weak and medium absorption range by means of two different models: the classical Cauchy formula and the single effective oscillator model proposed by Wemple and Di Domenico. From the latter theory, two physical parameters known as oscillator energy and oscillator strength, respectively, were obtained. These parameters have been related to the optical gap and structural properties of the deposited alloys. In the strong absorption region, the absorption coefficient and the optical gaps were calculated for each x-value. A quadratic trend was found for the x-dependence of the band gap, in agreement with the corresponding bulk alloy.

1. Introduction

II–VI Zn based ternary alloys are mostly important in the production of devices such as short wavelength emitting laser diodes and light emitting diodes [1–3]. One of the principal characteristic of these compounds lies in their non-linear optical properties. In fact, studies carried out on ZnSe since 1966 by Patel [4] gave interesting results on the second harmonic generation coefficient which was found to be 4×10^{-7} esu. When they are deposited as thin films, these alloys give also the possibility of tailoring devices showing band gap modulation. Furthermore, their electronic band structure and the wide range of band gap together with a low refractive index allow intense light transmission and also effective electron transport at high electric field. The interest in Zn based ternary alloys is also particularly concerned with the increasing demand for materials useful for the production of flat panel display, high efficiency electroluminescent and field emission devices. Nevertheless, they show a lower crystallinity, with respect to other semiconducting compounds; therefore they are highly defective and their structural properties are mainly linked to the growth processes used for the layer deposition.

Among the new and up to date techniques used for thin film deposition, pulsed laser ablation (PLA) is one of the most versatile methods to obtain layers of several materials that can be processed into a pellet target [5–11]. One of the important features of this method is based on the possibility of maintaining the stoichiometry of the ablated target in the deposited layer. In recent papers [12–15], our group has demonstrated the PLA capability of obtaining high quality II–VI Cd compounds on different substrates such as silicon, gallium arsenide and quartz.

In this work we report new results on the structural and optical properties of ZnS_xSe_{1-x} laser ablated films on quartz substrates. X-ray diffraction analysis was performed for structural characterization while the optical properties were studied at room temperature by transmittance and reflectance measurements. Particular attention was devoted to the calculation of the optical parameters such as energy gap (E_g) and absorption coefficient (α) whose calculation was done with the aid of well known methods and

‖ Corresponding author: Dr Vito Capozzi, Dipartimento di Fisica, Università di Bari, Via Amendola 173, I-70126 Bari, Italy. E-mail address: capozzi@ba.infn.it

0268-1242/98/121446+10$19.50

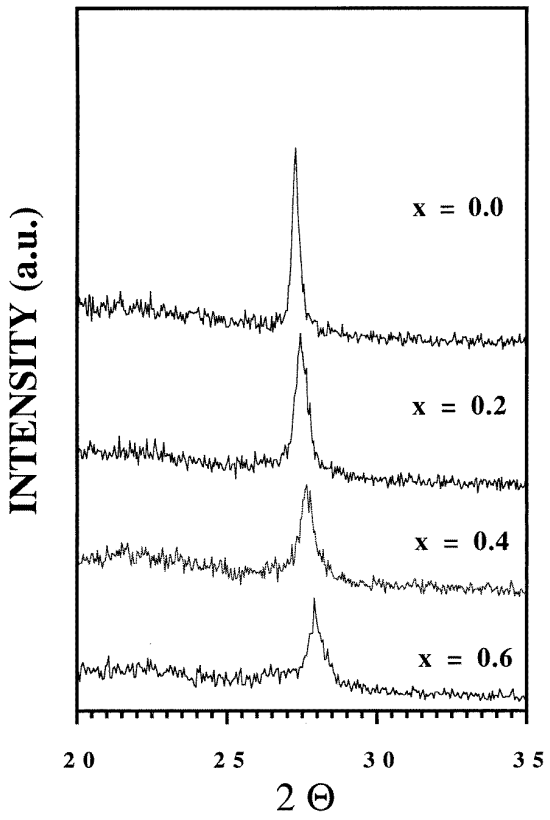

Figure 1. X-ray diffraction spectra of ZnS_xSe_{1-x} (x = 0.0, 0.2, 0.4, 0.6) films deposited on quartz substrates by laser ablation: a shift of the (111) peak can be noted when the sulphur concentration is increased. The compositions x = 0.8 and x = 1.0 are not reported because of a lack of film preferential orientation.

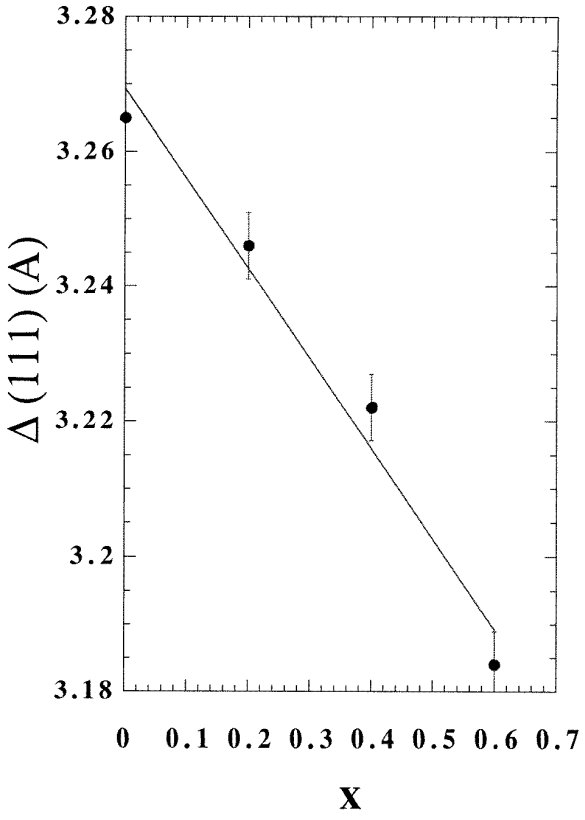

Figure 2. Plot of the interplanar distance $\Delta(111)$ against sulphur concentration x. $\Delta(111)$ has been obtained from the 2Θ angle of the x-ray diffraction peak. The Δ values are in agreement with those of [20] for the crystalline ternary alloys. The best straight line linking Δ to x is given by the following expression: $\Delta(111) = 3.269 - 0.133x$.

formulas. Moreover, the Swanepoel procedure [16–18] was specifically applied to deduce the values of the real part of the refractive index (n) and estinction coefficient (k).

2. Experimental procedure

ZnS_xSe_{1-x} films were deposited on clean quartz substrates by ablating stoichiometric home-made targets obtained by proper mixing and cold pressing high purity (99.999%) powders respectively of ZnS and ZnSe. The used x-values were x = 0.0, 0.2, 0.4, 0.6, 0.8 and 1.0. A pulsed Nd:YAG laser operating at 532 nm with a repetition rate of 10 Hz, and with a pulse width of 10 ns, was used as light source. The laser fluence was fixed at about 10 J cm^{-2} to allow the monolayer deposition, while the substrate temperature was optimized at 400 °C. The experimental set-up of the deposition system was described in a previous work [12]. Briefly, the substrate was placed in an evacuated stainless steel chamber (residual pressure of 10^{-6} mbar) and the laser beam was focused onto a rotating target at an oblique angle of 45° to allow the plume expansion in the direction normal to the target surface. The sample dimensions were 10×10 mm^2 and the thickness uniformity was evaluated to be over an area of 5×5 mm^2 by profilometer measurements. The surface of the deposited layer appeared uniform with no evidence of particulate deposition. This is in accordance with what is referred to in [19]: in fact, due to the high vapour pressure of the II–VI compounds at a temperature much below the melting temperature, the splashing penomena and consequently particulate depositions can be avoided. The target to substrate distance was fixed at 4 cm and the deposition time was 30 minutes for all samples, obtaining an average thickness of about 400 nm. X-ray analysis was performed by using a Θ–2Θ D5000 Siemens diffractometer. Room temperature transmittance and reflectance spectra were measured in the spectral range from 200 nm to 2500 nm using a Perkin-Elmer Lambda 9 double beam spectrophotometer.

3. Results and discussion

3.1. X-ray analysis

Figure 1 shows the x-ray diffraction spectra of ZnSSe thin films for different x-values (0.0, 0.2, 0.4 and 0.6). It can be remarked that the higher x the more the (111) oriented feature shifts from the ZnSe(111) to ZnS(111) oriented planes of the crystalline grains. As known from [9], thin films grow in the cubic phase (3C-zincblende structure)

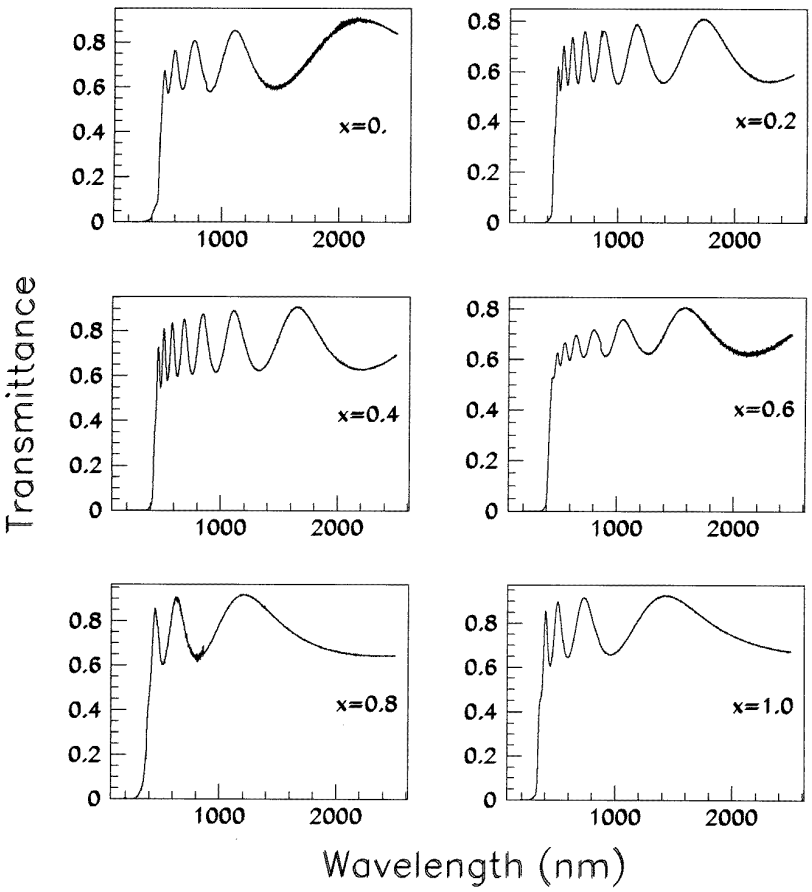

Figure 3. Transmittance spectra of ZnS_xSe_{1-x} films. The shift of the absorption edge is evident when the sulphur content is increased. A remarkable shrinking of the fringes can be observed for the composition $x = 0.6$.

on amorphous quartz substrates. In figure 2 the values of the interplanar distance $\Delta(111)$ are shown for the chosen x-value and this agrees perfectly with the corresponding distance found in the bulk alloys [20]. For x-values higher than 0.6, the films have a polycrystalline structure without the preferential (111) orientation. These features are typical of these compounds when they are epitaxially grown. In fact, the polycrystalline structure of the ZnS thin film has also been observed when the metal–organic chemical vapour deposition (MOCVD) technique is used [21].

3.2. Optical characterization at room temperature

3.2.1. Weak and medium absorption zone: calculation of the real and imaginary part of the refractive index. The real part of the refractive index was calculated starting from the transparent region, far from the absorption edge, by using the interpolating method. Such a procedure, which was first described by Valeev [22], basically uses transmittance spectra over which two interpolating curves enveloping maxima and minima of the interference fringes are superimposed. This problem was analytically solved by Swanepoel [16, 17] and Marquez *et al* [18] both in the case of uniform and non-uniform thin film thickness. As is well known [16], the expression of the thin film transmittance for normal incidence of the light is given by:

$$T = \frac{Ay}{B - Cy\cos\phi + Dy^2} \tag{1}$$

where $A = 16n^2s$, $B = (n+1)^3(n+s^2)$, $C = 2(n^2-1)(n^2-s^2)$, $D = (n-1)^3(n-s^2)$, $y = \exp(-\alpha d)$ and $\phi = 4\pi nd/\lambda$; s is the refractive index of the transparent substrate, d is the film thickness and λ is the wavelength of the light beam.

If the film thickness is uniform, the enveloping curves for the maxima and minima, respectively, are represented, as a continuous function of λ, by:

$$T_{M0} = \frac{Ay}{B - Cy + Dy^2} \text{ and } T_{m0} = \frac{Ay}{B + Cy + Dy^2}. \tag{2}$$

Therefore, n can be calculated at any wavelength by using the expression:

$$n = [N + (N^2 - s^2)^{1/2}]^{1/2} \tag{3}$$

where

$$N = 2s\frac{T_{M0} - T_{m0}}{T_{M0}T_{m0}} + \frac{s^2+1}{2}.$$

The non-uniformity in thickness can be observed in the spectra as a shrinkage in the transmittance fringes, whereas

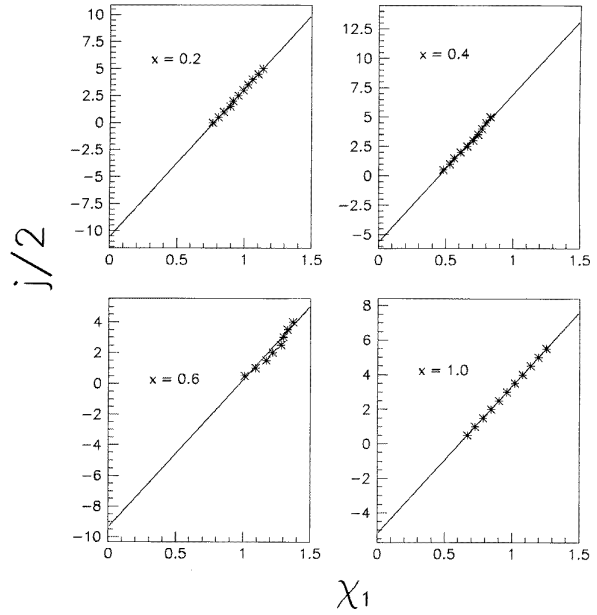

Figure 4. Plot of $j/2$ against χ_1 (symbols) for the compositions x = 0.2, 0.4, 0.6, 1.0. These data have been linearly fitted (full line) to equation (7) for the determination of the χ-values to be inserted in equation (4). The analytical expressions of the best straight lines are reported in table 1.

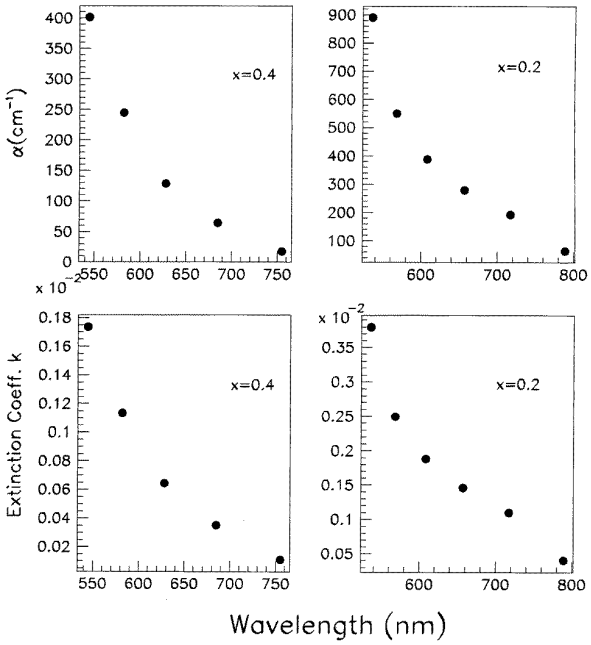

Figure 6. Examples of the trend of the absorption coefficient α and extinction coefficient k (dots) extrapolated in the weak and medium absorption range by using the expression linking the absorbance y to $n(\lambda)$ (see [17]). The results are shown for the composition x = 0.2 and x = 0.4.

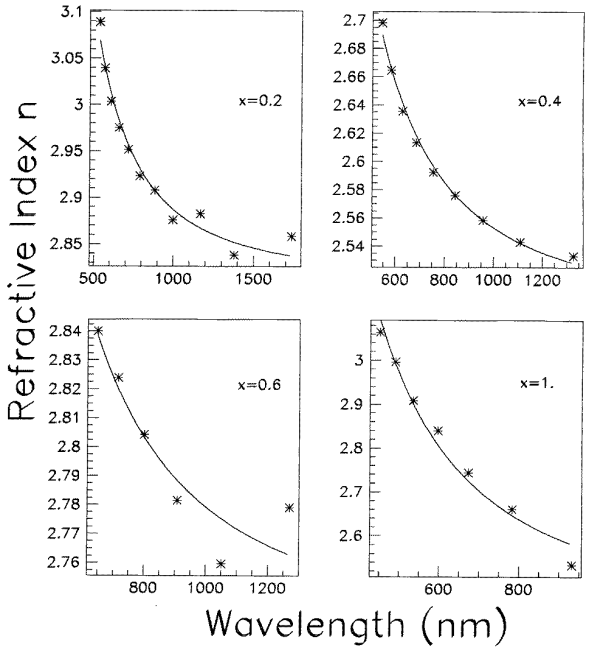

Figure 5. Plot of the refractive index (n) as a function of the wavelength for x = 0.2, 0.4, 0.6, 1.0: the plots show the n-values obtaining from the Swanepoel procedure [16, 17] and the fitting (full curve) was done with the classical Cauchy relation (see equation (9)). The expressions of the best curves are resumed in table 3.

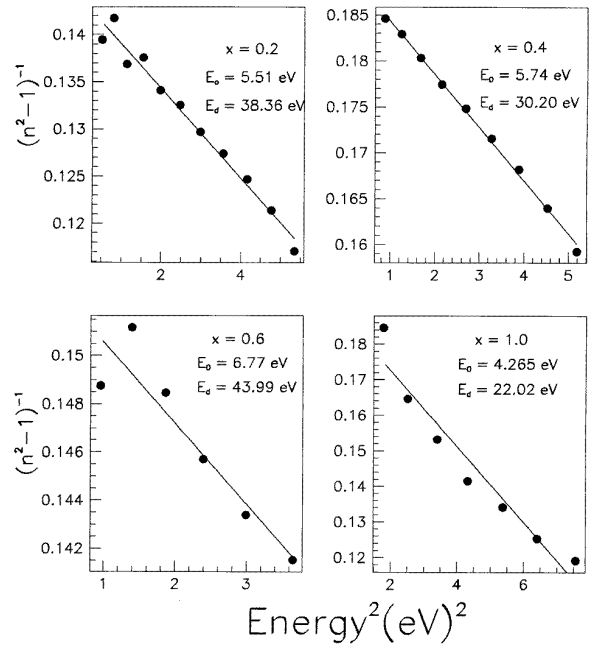

Figure 7. Plot of the refractive index factor $(n^2-1)^{-1}$ versus the square of the photon energy following the Wemple–Di Domenico model for four of the films studied [23, 24]. In the figure the experimental points are fitted to equation (12) (full line). The fitting values of the oscillator strength (E_0) and of the oscillator energy (E_d) are reported for each sulphur content (x).

their number is linked to the average thickness. These effects are introduced in the model by supposing that the film thickness varies linearly between $\langle d\rangle - \Delta d$ and $\langle d\rangle + \Delta d$, where $\langle d\rangle$ is the average thickness and Δd the thickness non-uniformity. Therefore the correct

analytical function representing maxima and minima in the transmittance spectra have to be obtained by integrating (1) over both Δd and y. In order to simplify this calculation, y has been approximated with an average value $\langle y\rangle = \exp(-\alpha\langle d\rangle)$, and the integration was carried out between $\varphi_1 = \langle d\rangle - \Delta d$ and $\varphi_2 = \langle d\rangle + \Delta d$. This choice is not detrimental for the final results if the constraint $\langle d\rangle \gg \Delta d$ is satisfied and α is almost constant in the examined spectral region. Finally, it can be shown that the above integration in the transparent region yields the following expressions of the envelope functions of the maxima and minima in the transmittance spectra:

$$T'_M = \frac{\sqrt{T_{m0}T_{M0}}}{\chi}\tan^{-1}\left[\sqrt{\frac{T_{M0}}{T_{m0}}}\tan^{-1}\chi\right]$$

$$T'_m = \frac{\sqrt{T_{m0}T_{M0}}}{\chi}\tan^{-1}\left[\sqrt{\frac{T_{m0}}{T_{M0}}}\tan^{-1}\chi\right] \qquad (4)$$

where T'_M and T'_m are the experimental envelopes of the non-uniform films, T_{M0} and T_{m0} are the envelopes of the uniform film whose thickness is equal to $\langle d\rangle$ and χ is a parameter given by:

$$\chi = 2\pi n\Delta d/\lambda \qquad \text{with } 0 < \chi < \pi/2. \qquad (5)$$

Equation (5) can be substituted in the following basic formula for the interference extrema:

$$2n\langle d\rangle = m\lambda \qquad (6)$$

where m is the order number of each interference extreme (integer for a maximum and half integer for a minimum). Equation (6) can be expressed as $2n\langle d\rangle = (m_1 + j/2)\lambda$ where m_1 is the order number of the first extreme considered starting from the long wavelength end of the spectra, and $j = 0, 1, 2, \ldots$. The substitution of (5) in (6) yields a more useful expression linking the maxima and minima orders to χ:

$$\frac{j}{2} = \left(\frac{\langle d\rangle}{\pi\Delta d}\right)\chi - m_1 \qquad \text{with } 0 < \chi < \pi/2. \qquad (7)$$

In order to extrapolate the value of T_{M0} and T_{m0} at the interference extrema, a rapid convergent algorithm (Newton–Raphson method) was adopted, following what is described in [16–18]. As a first approximation, in the transparent region it was supposed that $T_{M0} = T_s$, where T_s is the transmittance of the bare quartz substrate; by substituting these values in (4), the system of two transcendental equations can be solved by finding the corresponding roots (T_{m0}, χ) for the interference extrema. The order numbers ($m_1 + j/2$) are then related to the corresponding χ values. By linearly fitting the $j/2$–χ plot, it is possible to calculate the ratio $\langle d\rangle/\pi\Delta d$ and m_1. The best fitting straight line is used to obtain the corrected χ at the interference extrema. These results are then inserted in the formula (4) and the new unknown values, T_{M0} and T_{m0}, are obtained by applying the same algorithm as described before. Then, the first approximated values of the refractive index n_1 near all extrema are calculated by using the expression (3). The layer thickness can be deduced from the expression

$$d_1 = \frac{\lambda_1\lambda_2}{2(n_{12}\lambda_1 - n_{11}\lambda_2)} \qquad (8)$$

where n_{11} and n_{12} are the calculated refractive index at two adjacent maxima (or minima) at λ_1 and λ_2. The d_1 values have been then derived at each extremum and averaged. The final result is the first approximation of the average thickness $\langle d_1\rangle$ which is inserted in the interference condition expression $2n_1\langle d_1\rangle = m'\lambda$. This leads to the evaluation of the true order numbers m, which are obtained by appropriately rounding the m' values to integer or half integer numbers. The m values together with the n_1 ones are inserted in (6) in order to determine the d_2 values at each wavelength and the averaged corrected thickness $\langle d_2\rangle$. This result is used in (6) with the true order numbers m to obtain the corrected refractive index n_2 against λ. It has to be noted that $\langle d_2\rangle$ will be considered in the following as the film thickness in the calculation of the absorption coefficient.

Table 1. Best straight lines fitting the order number $j/2$ to χ_1. The χ_1-values have been obtained by using the Newton–Raphson algorithm and equations (4) as indicated in [17] and [18]. The straight lines have been used to extrapolate the χ-values used in the transcendental equations (4).

x	$j/2$
0.2	$-10.546 + 13.650\chi$
0.4	$-5.670 + 12.553\chi$
0.6	$-9.367 + 9.606\chi$
1	$-5.704 + 8.539\chi$

Figure 3 shows the transmittance spectra near the absorption edge and in the transparent region for ZnS_xSe_{1-x} thin films. It can be observed that the thickness of all films is almost uniform because the shrinking of the interference fringes is not remarkable, except that for $x = 0.6$. Nevertheless, due to the small number of fringes for $x = 0.8$ and $x = 0.0$, the n–λ trend will be shown only for $x = 0.2, 0.4, 0.6, 1.0$. In figure 4 are displayed the best straight lines relating $j/2$ to χ_1 whose analytical expressions are resumed in table 1.

In table 2 are illustrated all the results obtained with the Swanepoel procedure described above together with the evaluations of the thickness non-uniformity of the sample. It can be seen that, except that for $x = 0.6$, these values are all less than 20 nm, thus confirming the almost uniform in thickness. In the same table the averaged thickness $\langle d_1\rangle$ and $\langle d_2\rangle$ and their standard deviations are reported. In figure 5, the final values of the refractive index n_2 against λ have been plotted (symbols) and fitted (continuous lines) to the classical Cauchy expression:

$$n = a/\lambda^2 + b \qquad (9)$$

where a and b are material dependent constants. Equation (9) can be used to extrapolate n near the strong absorption region. The resulting analytical trends for each

Table 2. Values of I, T'_M and T'_m for four transmission spectra of ZnS_xSe_{1-x} films. T_{M0} and T_{m0} have been calculated from T'_M and T'_m (see equations (4)) by using the Newton–Raphson algorithm [17]. In the same table all the steps followed for the final calculation of the corrected refractive index n_2 are reported according to the procedure described in [17] and [18]. The values of non-uniformity Δd of the thin films are also indicated together with the corrected thickness d_2.

λ (nm)	T'_M	T'_m	T_s	$I/2$	χ_1	χ	T_{M0}	T_{m0}	d_1 (nm)	n_1	m_0	d_2 (nm)	n_2
ZnS: $\langle d_1\rangle$ = 390 nm, σ_1 = 54 nm, $\langle d_2\rangle$ = 368 nm, σ_2 = 29, Δd = 13 nm													
451	0.718	0.561	0.928	4	1.13	1.14	0.931	0.452		3.114	5	362	3.065
490	0.747	0.577	0.929	3.5	1.08	1.08	0.932	0.481		2.982	4.5	370	2.997
535	0.769	0.592	0.929	3	1.02	1.02	0.924	0.510	315	2.844	4	376	2.908
597	0.793	0.607	0.930	2.5	0.96	0.96	0.925	0.536	333	2.736	3.5	382	2.840
673	0.812	0.619	0.931	2	0.87	0.90	0.924	0.559	360	2.644	3	414	2.744
783	0.831	0.626	0.932	1.5	0.85	0.84	0.929	0.574	393	2.592	2.5	378	2.660
932	0.846	0.633	0.933	1.0	0.79	0.78	0.929	0.589	413	2.534	2	368	2.533
1155	0.862	0.640	0.932	0.5	0.73	0.73	0.933	0.601	436	2.499	1.5	347	2.354
$ZnS_{0.2}Se_{0.8}$: $\langle d_1\rangle$ = 566 nm, σ_1 = 30 nm, $\langle d_2\rangle$ = 607 nm, σ_2 = 18, Δd = 14 nm													
536	0.700	0.537	0.929	5	1.14	1.14	0.928	0.426		3.232	7	592	3.003
568	0.719	0.546	0.931	4.5	1.10	1.10	0.929	0.443		3.140	6.5	595	2.975
608	0.735	0.550	0.931	4	1.06	1.07	0.934	0.454	530	3.092	6	599	2.951
657	0.748	0.554	0.931	3.5	1.03	1.03	0.932	0.465	553	3.038	5.5	603	2.923
717	0.760	0.556	0.932	3	0.99	0.99	0.930	0.475	545	2.989	5	612	2.908
789	0.774	0.560	0.931	2.5	0.95	0.96	0.933	0.485	560	2.945	4.5	623	2.876
883	0.788	0.567	0.932	2	0.92	0.92	0.933	0.499	556	2.887	4	627	2.882
998	0.799	0.576	0.933	1.5	0.90	0.88	0.927	0.515	542	2.805	3.5	624	2.838
1167	0.812	0.577	0.932	1.0	0.85	0.85	0.931	0.521	571	2.793	3	635	2.858
1379	0.823	0.579	0.934	0.5	0.81	0.81	0.934	0.528	618	2.761	2.5	580	3.089
1736	0.835	0.581	0.935	0	0.77	0.77	0.937	0.535	611	2.734	2	588	3.039
$ZnS_{0.4}Se_{0.6}$: $\langle d_1\rangle$ = 631 nm, σ_1 = 17 nm, $\langle d_2\rangle$ = 655 nm, σ_2 = 8, Δd = 17 nm													
544	0.822	0.579	0.931	4.5	0.80	0.81	0.932	0.527		2.736	6.5	646	2.698
582	0.834	0.588	0.931	4	0.77	0.77	0.931	0.542		2.715	6	643	2.664
628	0.843	0.596	0.932	3.5	0.74	0.73	0.927	0.556	629	2.659	5.5	649	2.635
685	0.852	0.601	0.933	3	0.71	0.69	0.926	0.566	600	2.625	5	650	2.613
755	0.863	0.606	0.930	2.5	0.66	0.65	0.928	0.575	627	2.595	4.5	655	2.592
844	0.875	0.610	0.932	2	0.61	0.61	0.933	0.583	631	2.565	4	658	2.576
958	0.882	0.614	0.933	1.5	0.56	0.57	0.932	0.590	630	2.532	3.5	662	2.558
1111	0.889	0.618	0.930	1.0	0.53	0.53	0.932	0.598	648	2.519	3	662	2.543
1328	0.898	0.622	0.932	0.5	0.48	0.49	0.934	0.605	652	2.491	2.5	666	2.533
$ZnS_{0.6}Se_{0.4}$: $\langle d_1\rangle$ = 504 nm, σ_1 = 70 nm, $\langle d_2\rangle$ = 571 nm, σ_2 = 23, Δd = 59 nm													
649	0.695	0.602	0.931	3	1.30	1.29	0.931	0.461		3.056	5	531	2.840
717	0.705	0.608	0.932	2.5	1.28	1.25	0.895	0.490		2.881	4.5	560	2.824
801	0.747	0.639	0.933	2	1.22	1.19	0.887	0.505	406	2.798	4	573	2.804
908	0.735	0.612	0.932	1.5	1.17	1.14	0.913	0.534	487	2.717	3.5	585	2.781
1051	0.778	0.635	0.932	1	1.09	1.09	932	0.544	544	2.706	3	583	2.759
1270	0.803	0.642	0.932	0.5	1.01	1.04	0.947	0.558	562	2.670	2.5	595	2.779

composition are given in table 3. Moreover, it was also possible to deduce the absorbance y and, consequently, the absorption (α) and extinction (k) coefficients in the weak–medium absorption region. In fact, solving the equations (2) the final expression for y is given by [17]:

$$y = \frac{F - [F^2 - (n^2-1)^3(n^2-s^4)]^{1/2}}{(n^2-1)^3(n-s^2)} \qquad (10)$$

where $F = 8n^2s/T_i$ and $T_i = 2T_MT_m/(T_M+T_m)$.

Taking into account the dependence of y on α (see equation (1)), and by using n against λ in table 3, α and k were evaluated, with $k = \alpha\lambda/4\pi$. Some results are shown as an example in figure 6.

Besides the empirical Cauchy formula (9), an interesting model describing the n dispersion curve was proposed by Wemple and Di Domenico [23, 24]. This model consists in a proper evaluation of the real part of the dielectric constant $\varepsilon_1(\omega)$, that has the following formal expression:

$$\varepsilon_1(\omega) = 1 + \frac{4\pi e^2}{m_e\Omega}\sum_{\bar{k}}\frac{f^a_{cv}(\bar{k})}{\omega^a_{cv}(\bar{k}) - \omega^2} \qquad (11)$$

where e and m_e are respectively the electronic charge and mass, Ω is the volume of the crystal, c and v denote the conduction and valence bands, $\bar{k}$ is a Brillouin zone (BZ) vector, f^a_{cv} is the interband oscillator strength and ω^a_{cv} is the oscillator frequency. The Wemple–Di Domenico estimate of ε_1 is founded upon the hypotheses that (i) the important interband transitions in the BZ can be approximated by individual oscillators ω_n; (ii) the summation over oscillators can be approximated, for $\omega < \omega_n$, by a summation of the first strong oscillator and a proper combination of the higher order contributions in which only the terms to order ω^2 are retained. Consequently, a single effective oscillator model

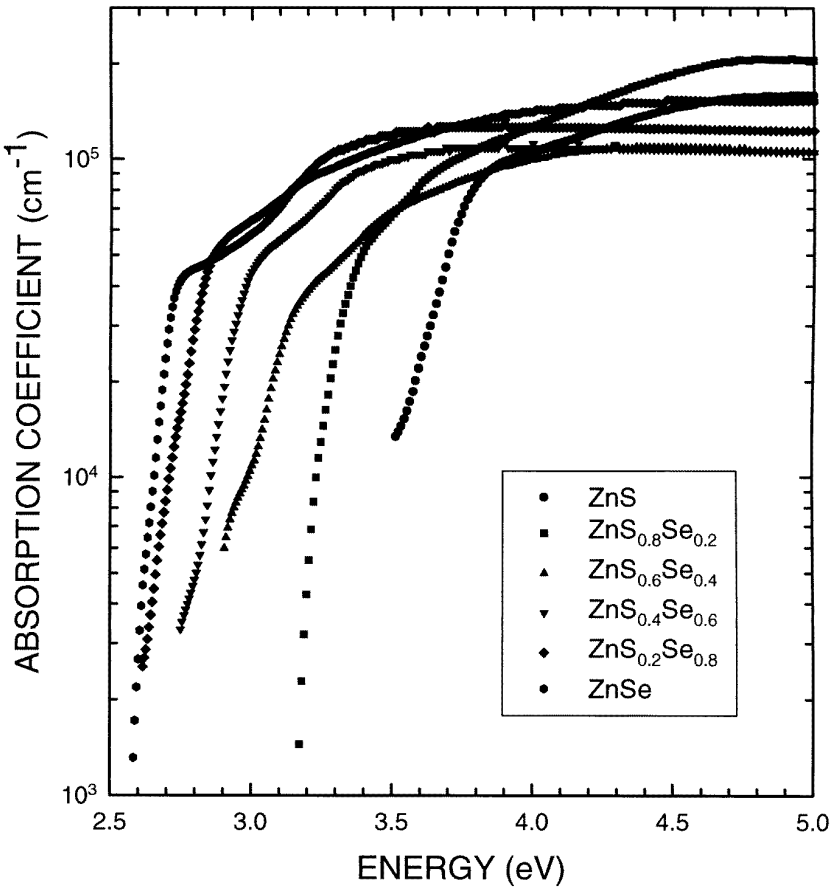

Figure 8. Semilogarithmic plot of the optical absorption coefficient as a function of the photon energy in the high absorption region for the ZnS_xSe_{1-x} films. The plots refer to different sulphur content (x) as illustrated in the legend. The absorption coefficient is calculated by equation (14).

of $\varepsilon_1(\omega)$ is obtained. It accounts for the n dispersion curve of several materials with a good accuracy, according to the following relation:

$$n^2(\hbar\omega) = 1 + \frac{E_d E_0}{E_0 - (\hbar\omega)^2} \tag{12}$$

where $\hbar\omega$ is the photon energy, E_0 and E_d are two parameters connected to the optical properties of the material: they are known as the single oscillator energy (E_0) and the oscillator strength (E_d). The former can be considered as an average energy gap and almost verifies the relation $E_0 = 2.3E_g^{opt}$. The latter is a measure of the average strength of the interband optical transitions. In particular, Wemple showed that E_d does not depend on either the bandgap or the volume density of the valence electrons, but it was found to obey the simple empirical relationship:

$$E_d = \beta N_c Z_a N_e. \tag{13}$$

In this formula N_c is the coordination number of the cation nearest neighbour to the anion, Z_a is the formal chemical valency of the anion and N_e is the effective number of valence electrons per anion. The coefficient β is a two valued parameter and it is an index identifying the chemical bonding in the crystalline structure. β could take values between the ionic one, which was estimated for halides and oxide as $\beta_i = 0.26 \pm 0.04$, and the covalent one $\beta_c = 0.37 \pm 0.05$ in zincblende, schelite and diamond-like structures. In our pure compounds, i.e. crystalline ZnS and ZnSe, the bond is strongly covalent and the β_c values are estimated to be 0.41 for ZnS and 0.42 for ZnSe [23].

Plotting $(n^2 - 1)^{-1}$ against $(\hbar\omega)^2$ it is then possible to obtain an experimental verification of (12): the best fit gives a straight line, whose angular coefficient and constant term depend on E_0 and E_d. The final results are shown in figure 7. In the legend are also reported the parameters E_0 and E_d obtained from our fit. It can be observed that in the intermediate compounds there is a general increasing trend of E_0 which is expected because of the relation linking E_g^{opt} to E_0. These values almost verify the approximate relationship $E_0 = 2E_g^{opt}$. The E_d values obtained for the intermediate compounds turned out to be larger than those of ZnS and ZnSe. It has to be pointed out that this effect on E_d has also been observed in other types of ternary alloys [18]. Similar to what is described in [18], even if the bond in our samples can be supposed to be strongly covalent, the slight increase in E_d has to be attributed to a higher number of nearest neighbours in the alloy with respect to the pure compounds. Our results showed that N_c assumes the following values: $N_c = 5.7$, 4.5 and 6.5

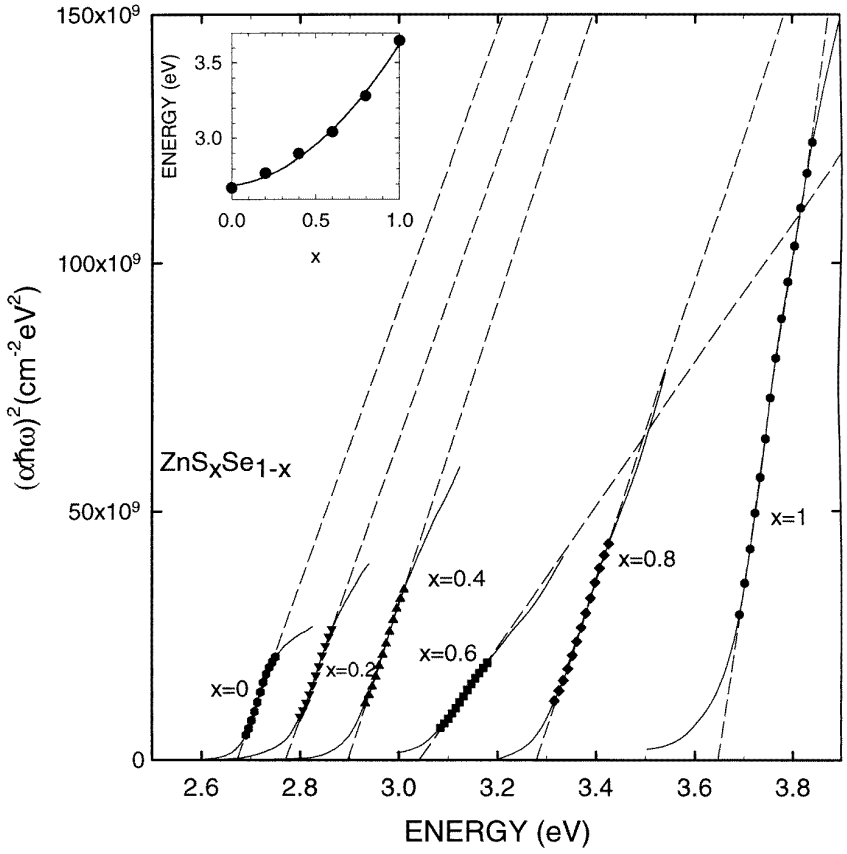

Figure 9. Plot of the $(\alpha\hbar\omega)^2$ factor versus the photon energy, in order to obtain the optical gap E_g^{opt}, according to the Tauc law (15), for all the examined samples. The experimental data (filled points) are fitted to equation (16) (dashed line), whose intercept with the horizontal axis yields the E_g^{opt} value. The inset displays the optical gap (filled points) versus sulphur content x in the ZnS_xSe_{1-x} films. The continuous line is a fit of the E_g^{opt} data to equation (16), giving the following parameters: $E_g(0) = 2.672 \pm 0.029$ eV, $E_g(1) = 3.279 \pm 0.029$ eV, $C = 0.805 \pm 0.133$ eV.

Table 3. Best fits of the experimental trend of the refractive index (n_2) against the wavelength λ for the four sample compositions (x) examined. The fitting has been obtained by using the well known Cauchy relation (equation (9)).

x	$n(\lambda)$
0.2	$\frac{7.435\times10^4}{\lambda^2} + 2.813$
0.4	$\frac{5.737\times10^4}{\lambda^2} + 2.346$
0.6	$\frac{4.331\times10^4}{\lambda^2} + 2.736$
1.0	$\frac{1.577\times10^5}{\lambda^2} + 2.346$

for $x = 0.2, 0.4, 0.6$ respectively. This could be basically due to the presence of atoms which do not perfectly act as substitutional in the crystalline structure of the deposited layer. As for the ZnS film, we found a value of E_d almost in agreement with that calculated in the crystalline ZnS (22 eV), while E_0 is equal to 1.2 times the optical gap.

3.2.2. Region of strong absorption: energy gap and absorption coefficient. From transmittance and reflectance spectra the dependence of the absorption coefficient on the photon energy near the absorption edge can be obtained. Taking into account multiple reflection the following expression yields the transmittance T (for normal incidence of the light beam on the sample surface), in a spectral region where interference effects may be neglected and $k \ll n$ (which is true for most transmission experiments) [25]:

$$T = \frac{(1-R)^2\exp(-\alpha d)}{1-R^2\exp(-\alpha d)} \tag{14}$$

where R is the sample reflectivity at normal incidence. Thus, α can be evaluated from transmission and reflectance measurements, by using the above expression, where the $\langle d_2\rangle$-value is used for the thickness of the sample. The calculated α-values are shown in figure 8 for all the examined ZnSSe epilayers. The blue shift of the absorption edge is clearly visible with increasing sulphur content, due to the rising of the energy gap. In the spectral region of strong absorption ($\alpha > 10^4$ cm^{-1}) the optical gap E_g^{opt} is defined according to [26]:

$$\alpha(\hbar\omega)\hbar\omega = A(\hbar\omega - E_g^{opt})^r \tag{15}$$

where A is a constant and r is a number which characterizes the transition process: r has a value of 1/2 for the direct

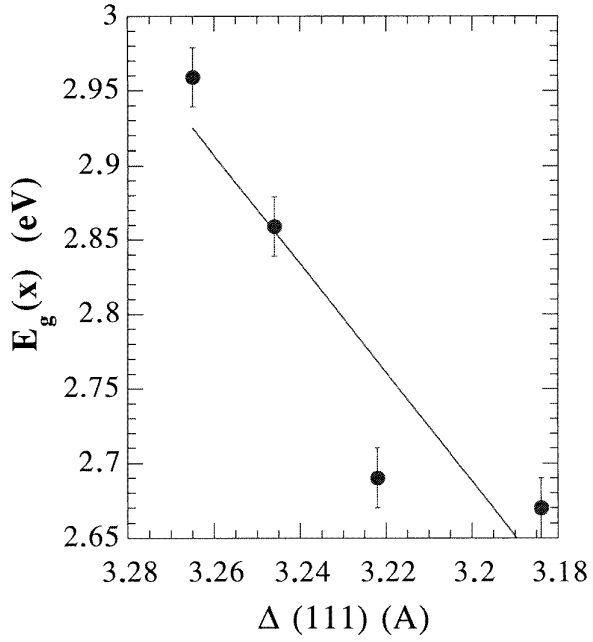

Figure 10. Plot of the energy gap (E_g^{opt}) as a function of the interplanar distance $\Delta(111)$. A linear least squares fit has been performed (full line) up to a composition $x = 0.6$ where preferential orientation of the grains was observed. The fitting straight line is expressed by the equation: $E_g^{opt} = 15.250 - 3.857\Delta(111)$.

allowed transition. This relationship is valid for parabolic valence and conduction bands near the band gap and for transition elements equal for all transitions.

The linear dependence of $(\alpha\hbar\omega)^2$ on the photon energy for the ZnS_xSe_{1-x} films, shown in figure 9, indicates the existence of a direct transition in the strong absorption region. In addition, if we assume that the band gap E_g corresponds to the E_g^{opt} value, a linear extrapolation of the graph of $(\alpha\hbar\omega)^2$ versus $\hbar\omega$ (dashed lines in figure 9) yields the energy gap for each x composition of the film. Such E_g values are in good agreement with those in the literature [20].

The dependence of the energy gap of a ternary alloy on the composition x at a fixed temperature can be described by the empirical equation [27]:

$$E_g(x) = E_g(0)(1-x) + E_g(1)x - Cx(1-x) \qquad (16)$$

where $E_g(0)$ and $E_g(1)$ are the fundamental band gaps of the binary compounds and C is the non-linear (or 'bowing') parameter. This quadratic dependence has been verified for our ZnS_xSe_{1-x} epilayers, by a least squares fitting of the E_g^{opt} values: the obtained $E_g(0)$, $E_g(1)$ and C parameters are reported in the figure caption. As previously stated the values of the optical band gap almost verify the relationship $E_0 = 2E_g^{opt}$. In the inset of figure 9, the dependence of the energy gap on the sulphur concentration is represented. Finally, the linear dependence of the energy gap on the interplanar distance, shown in figure 10, allows us to relate the structural parameters to the optical ones.

4. Conclusions

In this paper we reported new results on the structural and optical characterizations of laser ablated ZnS_xSe_{1-x} thin film on quartz substrates. The deposited layers show a good degree of crystallinity up to a composition of $x = 0.6$, despite the amorphous nature of the substrate. For larger composition the crystallographic quality is not excellent even if the optical parameters show a good agreement with the expected ones for bulk alloys. The good optical properties allowed us to calculate the absorption coefficient, the refractive index and extinction coefficient in the whole spectral range from the absorption edge to the transparent optical zone. Moreover, it was also possible to use a classical model to obtain information on the chemical bond and quality of the crystalline structure and strength of the interband transition. From these results it can be noted that the ablated film almost maintains the stoichiometry of the target. More work is still in progress in our laboratories to improve the crystallinity of ZnS and $ZnS_{0.8}Se_{0.2}$ thin films even if their room temperature optical response is comparable with that of the corresponding bulk materials.

In conclusion, our results are a proof of the great advantage offered by this low cost technique with respect to other sophisticated methods such as MBE and MOCVD. The possibility of maintaining in the laser deposited films the stoichiometry of the target (which is simply made of separate but appropriately mixed powders without any other treatment) allows us to conclude that PLAD can be considered in perspective an alternative technique to evaporative, rf or more expensive methods for depositing high quality thin films or superlattices of these interesting optoelectronic compounds.

References

[1] Hasse M A, Qiu J, De Puydt J J M and Cheung H 1991 *Appl. Phys. Lett.* **59** 1272
[2] Jeon H, Ding J, Patterson V, Nurmikko A V, Xie W, Grillo D C, Kobayashi M and Gunshor R L 1991 *Appl. Phys. Lett.* **59** 3619
[3] Okuyama H, Miyajima T, Morinaga Y, Hiai F, Ozawa M and Akimoto K 1992 *Electron. Lett.* **28** 1798
[4] Patel C K N 1966 *Phys. Rev. Lett.* **16** 613
[5] Giardini-Guidoni A, Di Palma T M, Teghil R, Marotta V, Ambrico M, Piccirillo S and Orlando S *Surf. Cat. Technol.* at press
[6] Venkatesan T, Wu X D, Inam A and Wachtman J B 1988 *Appl. Phys. Lett.* **52** 1095
[7] Kwok H S, Zheng J P, Witanachi S, Mattoks P, Shi L, Ying Q Y, Wang X W and Shaw D T 1988 *Appl. Phys. Lett.* **52** 1095
[8] Kwock H S, Zheng J P, Witanachchi S, Shi L and Shaw D T 1988 *Appl. Phys. Lett.* **52** 1815
[9] Shen W P and Kwok H S 1994 *Appl. Phys. Lett.* **65** 2162
[10] Cheung J T, Niizawa G, Moyle J, Ong N P, Pain B M and Viceand T 1986 *J. Vac. Sci. Technol.* A **4** 2086
[11] Norton M G, Kotula P G and Carter C B 1991 *J. Appl. Phys.* **70** 2871
[12] Ambrico M, Smaldone D, Martino R, Perna G, Capozzi V and Giardini A 1997 *Mater. Sci. Eng.* B **43** 102
[13] Giardini A, Ambrico M, Smaldone D, Martino R, Parisi G, Capozzi V and Perna G 1996 *Appl. Surf. Sci.* **106** 144
[14] Perna G, Capozzi V, Ambrico M, Smaldone D and Martino R 1997 *J. Lumin.* **72–74** 90

[15] Perna G, Capozzi V, Ambrico M, Smaldone D and Martino R 1998 *J. Lumin.* **76–77** 534
[16] Swanepoel R 1984 *J. Phys. E: Sci. Instrum.* **17** 896
[17] Swanepoel R 1983 *J. Phys. E: Sci. Instrum.* **16** 1214
[18] Marquez E, Gonzalez-Leal J M, Jimenez-Garay R, Lukic S R and Petrovic D M 1997 *J. Phys. D: Appl. Phys.* **30** 690
[19] Cheung J T 1994 *Pulsed Laser Deposition of Thin Films* ed D B Chrisey and G K Hubler (New York: Wiley) p 14
[20] *Landolt–Börnstein New Series* vols 17, 17b, ed O Madelung, M Schultz and H Weiss (Berlin: Springer)
[21] Leo G, Lovergine N, Prete P, Longo M, Cingolani R, Mancini A M, Romanato F and Drigo A V 1996 *J. Crystal Growth* **159** 144
[22] Valeev A S 1963 *Opt. Spectrosc.* **15** 500
[23] Wemple S H and Di Domenico M 1971 *Phys. Rev.* B **7** 1338
[24] Wemple S H 1973 *Phys. Rev.* B **7** 3767
[25] Abelès F 1972 *Optical Properties of Solids* ed F Abelès (Amsterdam: North-Holland) pp 21–92
[26] Tauc J, Grigorovici R and Vancu A 1966 *Phys. Status Solidi* a **15** 627
[27] Lunz U, Schumacher C, Nurnberger J, Schull K, Gerard A, Schusser U, Jobst B, Faschinger W and Landwehr G 1997 *Semicond. Sci. Technol.* **12** 970